nature cities

Article

https://doi.org/10.1038/s44284-024-00102-z

# Widespread global exacerbation of extreme drought induced by urbanization

Received: 29 February 2024

Accepted: 9 July 2024

Published online: 07 August 2024

Check for updates

Shuzhe Huang[1], Siqi Wang[2], Yuan Gan[1], Chao Wang[1] ✉, Daniel E. Horton[3], Chuxuan Li[3], Xiang Zhang[2], Dev Niyogi[4], Jun Xia[5] & Nengcheng Chen[1,2,6] ✉

Urbanization exerts considerable impact on ecological, environmental and meteorological processes and systems. However, the effects of urbanization on local drought remain under-explored. Here we characterize the effects of urbanization on drought across the world's cities using global weather station observations. We find that drought severity has increased at ~36% of global sites, while the extreme (less than a fifth) Standardized Precipitation Evapotranspiration Index has increased at ~43% of the city sites globally. We investigate the primary driving mechanisms behind drought exacerbation using physics-based weather research and forecasting model simulations. We find that urbanization induced warmer and drier urban environments, which has suppressed light rainfall and aggravated extreme local drought conditions. Furthermore, mid-twenty-first century CMIP6 projections indicate that nearly 57 and 70% of urban regions would consistently suffer exacerbated drought severity and extreme Standardized Precipitation Evapotranspiration Index due to urban expansion. Our findings highlight cities causing rainfall extremes and call for heightened attention to urban drought preparedness in the face of continued urbanization, population growth and climate change.

Drought is one of the Earth system's most profound and impactful extremes and has brought far-reaching consequences and cascading impacts across the globe, including ecological imbalances, water cycle degradation, food insecurity, economic losses and societal upheaval[1–3]. Traditionally, drought can be classified into four types, including meteorological drought (precipitation and atmospheric moisture deficit), agricultural drought (rainfall and soil moisture deficit), hydrological drought (surface runoff/groundwater and streamflow deficit) and socio-economic drought (deficit in water leading to societal impacts). In the context of ongoing global warming, aridity—characterized by inadequate atmospheric moisture supply and escalating water demand—has exhibited an increasing trend[4,5]. Recent studies have provided robust evidence linking the increased frequency and severity of drought to anthropogenic activities, with a particular emphasis on greenhouse gas emissions over the past half century[6,7]. However, as one of the most representative and apparent human activities, urbanization and its implications on local drought have also raised considerable concerns due to the growing population in cities in the Anthropocene epoch[8–10]. While some reports mention the potential association between urbanization and drought development[11,12], responses of local drought (especially meteorological drought) to urbanization still lack quantitative evidence and mechanistic understanding, particularly at global scales.

[1]State Key Laboratory of Information Engineering in Surveying, Mapping and Remote Sensing (LIESMARS), Wuhan University, Wuhan, China. [2]National Engineering Research Center of Geographic Information System, School of Geography and Information Engineering, China University of Geosciences (Wuhan), Wuhan, China. [3]Department of Earth and Planetary Sciences, Northwestern University, Evanston, IL, USA. [4]Department of Earth and Planetary Sciences, Jackson School of Geosciences, Maseeh Department of Civil, Architecture, and Environmental Engineering, University of Texas at Austin, Austin, TX, USA. [5]State Key Laboratory of Water Resources Engineering and Management, Wuhan University, Wuhan, China. [6]Hubei Luojia Laboratory, Wuhan, China. ✉e-mail: c.wang@whu.edu.cn; cnc@whu.edu.cn

Extensive efforts have been dedicated to investigating urbanization-induced alterations to local water cycles and meteorology[13,14]. Based on the Clausius–Clapeyron relation, the water vapor holding capacity of the atmosphere increases ~6–7% for every 1 °C increase in temperature. This theoretical relationship partly explains the intensified extreme rainfall and the increased frequency of flooding events in a warming climate[15]. In cities, it is widely recognized that urbanization transforms urban landscapes into heat-absorbing surfaces (for example, buildings, streets), creating locally warmer conditions, also known as the urban heat island (UHI)[16,17]. As warming drives variations in rainfall, enhanced heavy rainfall in urban regions has been widely observed and investigated[18–20]. Specifically, the UHI-thermal perturbation can cause destabilization of the boundary layer and result in downstream translation of the UHI circulation[21]. In addition, the UHI may also generate localized convection with the enhanced surface roughness and further intensify extreme rainfall[22,23]. Conversely, urbanization is also likely to cause changes in surface atmospheric humidity between urban and rural areas, compounded by the removal of vegetation, which reduces urban evapotranspiration[16,24].

In light of these dynamics, we propose that urbanization may also exert substantial influence on the development of local drought conditions. However, current knowledge concerning the attribution of drought development mainly focuses on large-scale forcings at regional to global scales, while the understanding of the impact of urbanization on local drought remains limited. Although urban regions are local in scale and only occupy ~3% of Earth's surface, nearly ~50% of the total population lives in cities, a number projected to reach 68% by 2050 (ref. 25). The dense concentration of population and frequent anthropogenic alterations in urban environments has made profound impacts on the water cycle and ecosystems at local to global scales[10,14]. For instance, ref. 26 delved into the causes of atmospheric dryness over 25 large urban agglomerations in the world and highlighted the role of urbanization in modifying local humidity through evapotranspiration. Reference 27 also highlighted the significance of considering urban development in projecting compound climate extremes[27]. Nevertheless, there is still a lack of global-scale quantitative understanding regarding whether and to what extent urbanization exacerbates or mitigates local drought.

Water resources in urban areas are generally controlled by a mix of local climate and hydrologic systems[28]. Specifically, local climate systems determine the water balance from precipitation, evapotranspiration and infiltration, while hydrologic systems control water availability by accounting for the transfers of surface and subsurface water[29]. The occurrence of urban drought disrupts the balance between local water supply and demand. For instance, decreased precipitation may reduce the inflows to surface water reservoirs, causing groundwater compensation, resulting in groundwater declines. Consequently, cities must adapt their water management strategies to deal with changing conditions. Indeed, many world cities such as Cape Town and São Paulo have faced or are facing a countdown to 'Day Zero', when cities can no longer afford to supply water to their residents[30]. Reference 31 also pointed out that future drought is likely to aggravate urban inequalities, public health and related water crises. Given these motivations, investigating the effects and driving mechanisms of urbanization on the extent and distribution of city-level drought is an essential step towards sustainable urban development and planning.

Here, we provide a quantitative analysis of the effects of urbanization on local drought development based on local observations and model simulations. We explore urbanization-induced changes in different drought characteristics (that is, duration, severity) and intensity levels (that is, extreme, heavy, moderate and light)[32]. The associations between urbanization and various drought metrics are quantified through the lens of trend differences between urban–rural pairs. By examining the spatial and temporal distributions of urbanization effects on each drought metric for global urban–rural pairs, we identify the major associations between urbanization and local drought. To further elucidate how drought responds to urbanization, we apply the weather research and forecasting (WRF) high-resolution regional atmospheric model to simulate local drought under highly urbanized scenarios (URB) and non-urbanized scenarios (NOURB) in six representative cities spread across each continent. Subsequently, we delve into the potential mechanisms underlying the effects of urbanization. Thus, our study is guided by three primary research questions:

(1) What associations exist between urbanization and local drought development across the globe?
(2) How does urbanization lead to local drought modification in cities?
(3) Will the detected urbanization effects persist in the future?

By addressing these questions, our findings enhance our understanding of the role of urbanization in shaping drought patterns—a critical step towards sustainable and informed urban development.

## Results

### Historical changes in local drought due to urbanization

To identify the potential associations between urbanization and local drought, we quantify the effects of urbanization on local drought using both in situ (station-scale) and ERA5-Land reanalysis (city-scale) data. We characterize local drought using six drought metrics, including four annual sums of SPEI with varying intensity levels (extreme (<5th percentile), heavy (5th–10th percentile), moderate (10th–20th percentile) and light (20th–30th percentile) SPEI) and two drought characteristics (duration and severity)[32]. Here, drought duration (length of a drought event) and drought severity (cumulative negative SPEI values during a drought event) are extracted using run theory on SPEI (flowchart in Supplementary Fig. 3). To minimize the impacts of potential regional confounding factors and further quantify the effects of urbanization on the six drought metrics, we perform urban–rural analyses at two scales. For station-scale analyses, we pair urban in situ stations with rural stations within a 100 km buffer (Methods). For city-scale analyses, we define urban regions using the urban boundaries provided by the Global Urban Boundary (GUB) dataset[33]. Corresponding rural regions are defined as the outward buffers of the urban boundaries using approximately the same land areas as contained within the urban boundaries[34]. To ultimately assess the effects of urbanization on local drought, for urban–rural station- and city-scale pairs, we compute the difference of each paired urban and rural drought metric trend: when negative and significant ($P < 0.050$), we describe urbanization as exacerbating drought, when positive and significant ($P < 0.050$), urbanization has mitigated drought and when statistically indistinguishable, we indicate no discernible relationship.

We calculate the proportions of stations and cities with each type of urbanization effect for six drought metrics (Fig. 1a,b). We find notable discrepancies in the effects of urbanization on different drought intensity levels of SPEI. At the station scale, we find that urbanization exerts a limited impact on light and moderate drought (SPEI), with the percentages of positively and negatively affected stations lower than 10%. However, a different distribution emerges for heavy SPEI, where urbanization shows a negative relationship with heavy SPEI at 15.94% of stations (nearly three times the number of positively affected stations). Such different effects of urbanization are most pronounced for extreme SPEI and drought severity. Specifically, urbanization is found to significantly worsen extreme SPEI and drought severity for around 43 and 36% of the stations worldwide, which are about five and four times the number of positively affected stations, respectively. We also examine the sensitivity of the quantitative results to the buffer distance during urban–rural pairing (Supplementary Fig. 4). Results obtained using 50 and 150 km buffer distances align with the 100 km-based results in Fig. 1a. City-scale results share similar

https://doi.org/10.1038/s44284-024-00102-z

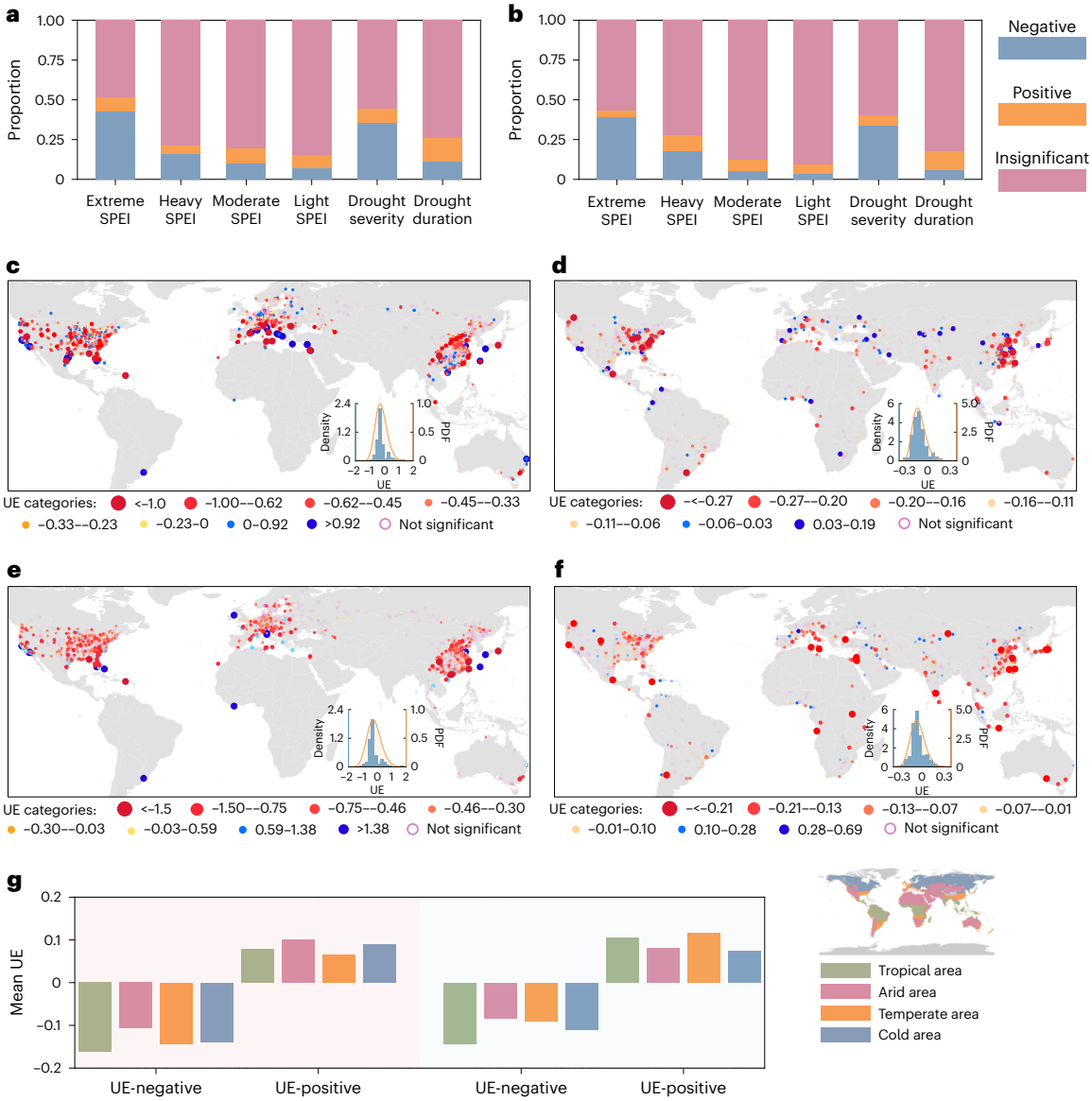


**Fig. 1 | Urbanization effects on various drought metrics. a**,**b**, The proportions of stations (**a**) and cities (**b**) with different types of urbanization effect (UE) for the six drought metrics using a 100 km urban–rural buffer threshold. Blue, orange and red bars represent the stations and/or cities with statistically significant negative UE, statistically significant positive UE and insignificant UE, respectively. **c**–**f**, The spatial distributions of UE on extreme SPEI and drought severity across world's stations and cities. The subfigures show the statistical distributions of the UE. Here, the negative and/or positive UE represents that urbanization exacerbates and/or mitigates drought conditions: distribution of UE on extreme SPEI (station) (**c**), distribution of UE on extreme SPEI (city) (**d**), distribution of UE on drought severity (station) (**e**) and distribution of UE on drought severity (city) (**f**). **g**, The UE on extreme SPEI and drought severity across four different climate zones based on the city-scale data, respectively. In this case, the negative UE and positive UE are visualized separately.

patterns with station-scale results, where roughly 39.1 and 33.7% of cities demonstrate urbanization-induced exacerbations on extreme SPEI and drought severity (Fig. 1b).

To gain deeper insights into the distinct urbanization effects on extreme SPEI and drought severity, we conduct a more exhaustive analysis on their spatial distributions (Fig. 1c–f). In general, stations with aggravated extreme SPEI and drought severity due to urbanization are distributed widely across the globe, particularly concentrated in the western United States and eastern China. The city-scale distributions (Fig. 1d,f) provide more detailed results in South America, Africa and central Asia, where limited in situ stations are available. The results show that the negative urbanization effects are also notable in southern South America, southern Africa and India. Among four climate zones, the tropical region exhibits the most pronounced negative urbanization effects on extreme SPEI and drought severity, followed by arid and temperate climate areas (Fig. 1g). By continents, the urbanization effects are more pronounced in Asia, North America and Africa (Supplementary Fig. 5). To analyse the potential influencing factors of the effects, we quantify the effects of urbanization on several drought-related factors, including precipitation, temperature, vapor pressure deficit (VPD) and enhanced vegetation index (EVI; Supplementary Fig. 6). The average urbanization effects on precipitation and temperature are negative and positive, respectively, for stations with negative urbanization effects on drought, indicating a decrease in precipitation and enhanced UHI with urbanization. In addition, urbanization is associated with increased VPD, which could pose challenges for local water availability and atmospheric humidity[35]. Meanwhile, the loss of vegetation often associated with urbanization further decreases urban evapotranspiration, resulting in the intensification of local atmospheric dryness (Supplementary Fig. 6d).

Conversely, the positively affected stations and cities, that is, locales where urbanization reduces drought severity, are scattered across continents, particularly coastal areas such as the western United States, Mediterranean and eastern Australia. To examine the potential coastal effects on urbanization-induced drought changes, we analyse the relationship between urbanization and distance to the coastline (Supplementary Fig. 7). We observe that the coastal effects are more prominent for cities with positive urbanization effects, of which urbanization-induced drought mitigation is more pronounced for coastal cities, especially in temperate and arid regions.

We further analyse patterns of urbanization effects by subdividing cities for different areal extents, vegetation cover and urbanization intensities. Here the cities are classified into small, medium, large and mega according to 0–25th, 25th–50th, 50th–75th and 75th–100th percentiles of urban areas, respectively. Similarly, vegetation cover is characterized by average EVI for each city and classified into low, medium, medium-high and high according to 0–25th, 25th–50th, 50th–75th and 75th–100th percentiles of EVI. For both extreme SPEI and drought severity, urbanization effects generally enhance with increasing city areas (Supplementary Fig. 8a,b). In other words, large and mega cities are prone to more considerable exacerbation of local drought than smaller cities (with average urbanization effects on extreme SPEI and drought severity of −0.149 and −0.092, and −0.090 and −0.023 for mega and small cities, respectively). Urbanization effects on local drought also vary according to the average vegetation cover for cities (Supplementary Fig. 8c,d). Specifically, cities with low vegetation density are found to have more extreme SPEI (−0.140) and drought severity (−0.089): trends probably attributable to, and in some cases a result of, the reduced cooling effect and evapotranspiration from vegetation[36]. Additionally, we analyse the relationship between urbanization effects and urbanization intensity characterized by the percentage of impervious surface area within a 2 km buffer for each station (Supplementary Fig. 9). We observe that higher urbanization intensity leads to greater extreme SPEI and drought severity with linear slopes of −0.0015 ($P < 0.050$) and −0.0008 ($P < 0.100$), respectively.

We also analyse the effects of urbanization on seasonal variations of drought and drought event frequency. We find that the effect of urbanization on drought exhibits substantial seasonality, with the most prominent negative effects during warm seasons, such as summer and negligible effects in winter (Supplementary Fig. 10). Further, we use return periods to characterize the drought frequency, which represents the time interval between drought events. We calculate the drought return period based on the joint distribution of drought duration and drought severity modeled by a copula function (Methods). Given drought events with the same duration and severity, urban regions exhibit shorter return periods compared to rural regions (Supplementary Fig. 11). In other words, urban areas are at a heightened risk of experiencing a given magnitude or intensity of drought event. For more detailed drought frequency results, refer to Supplementary Text 1 and Supplementary Fig. 11.

To examine uncertainties in the quantitative results, we conduct a series of sensitivity tests using different SPEI time scales (daily to monthly scales) and calculation units (station to grid cell units). Overall, results from these comparative tests provide additional corroborating evidence of the exacerbating effects of urbanization on extreme SPEI and drought severity (Supplementary Text 2 and Supplementary Figs. 12 and 13).

## Potential mechanistic explanation

To advance our understanding of how urbanization leads to the exacerbation of drought in cities, we use WRF simulations to model local drought evolution and evaluate the changes in drought between two urbanization scenarios: a URB and a NOURB. The simulations are performed in six representative urban clusters across different continents due to their notable urban expansion and historical severe drought occurrences[31,37–39]. The six urban clusters are the Yangtze River Delta (YRD) urban cluster in Asia, Madrid urban cluster in Europe, Illinois–Wisconsin–Indiana (IWI) urban cluster in North America, the São Paulo urban cluster in South America, Cape Town urban cluster in Africa and the New South Wales (NSW) urban cluster in Australia (Fig. 2a). By validating against local observations, the WRF simulations successfully reproduce observed meteorological variations (Supplementary Text 3 and Supplementary Figs. 14 and 15).

To characterize the urbanization effects on local drought conditions, we calculate the change in drought metrics between the URB and NOURB scenarios. By replacing impervious grid cells with vegetated grid cells, urban regions experience substantial changes in drought conditions (Fig. 2b). Substantial increases in extreme SPEI are observed across all regions, with average change rates substantially greater than zero, indicating an exacerbation of drought conditions due to urbanization. Prominent urbanization effects are identified in the São Paulo urban cluster and the YRD urban cluster, with average change rates of 8.8 and 6.3%, followed by the IWI urban cluster (5.5%), NSW urban cluster (3.5%), Cape Town urban cluster (2.9%) and Madrid urban cluster (2.8%). Changes in drought severity show similar patterns to extreme SPEI, where the YRD and São Paulo urban clusters experience an exacerbation of 3.7 and 3.3%, respectively, under URB conditions. Results for other drought indices can be found in Supplementary Fig. 16.

We assume that the drought changes in urban regions between the URB and NOURB scenarios can be primarily attributed to urbanization-induced modifications on local meteorological and hydrological processes. Thus, we analyzed the changes of several drought-related hydrometeorological factors between the URB and NOURB scenarios, aiming to explore potential mechanisms underlying urbanization-induced drought exacerbation. Urbanization typically involves replacement of cropland and vegetated areas with impervious surfaces, substantially affecting local water and energy balances[35,40]. Notably, we observe a change rate of 7.3% in air temperature from the NOURB to URB scenario, demonstrating the well-documented UHI effect (Fig. 3). Reduction of vegetated regions (that is, forest, cropland) also decreases latent heat flux for 509.33 W/m$^2$ in average over six urban clusters (with an average change rate of −87.1% in WRF simulations), which hampers water vapor exchange and evapotranspiration[41,42]. The expansion of impervious surface modifies soil heat capacity and infiltration rates, leading to elevated sensible heat flux for 326.89 W/m$^2$ in average (with an average change rate of 75.2% in WRF simulations)[43]. The cumulative impact of these factors amplifies VPD (with an average change rate of 44.9%), increases potential evapotranspiration (PET) (with an average change rate of 6.7%) and diminishes relative humidity (with an average change rate of −9.98%), ultimately creating drier conditions within cities: also known as the urban dry island (UDI) effect[26,44–46]. The heightened VPD and drier urban environment can create conditions that are not conducive for rainfall and suppress light rainfall (with an average change rate of −2.8%), resulting in support for drought to sustain[32]. According to the combined effects of the urbanization-induced factors, we find that extreme SPEI and drought severity are exacerbated by 6.2 and 3.6% between the URB and NOURB scenarios.

## Future projection of drought development under urbanization

Building on historical evidence that underscores the prominent negative effects of urbanization on extreme SPEI and drought severity, we extend our investigation to project the effects of future urbanization. Considering the relatively coarse spatial resolution of standard CMIP6 models, our analysis is conducted using HighResMIP models that simulate the Shared Socioeconomic Pathway (SSP) 5-8.5 scenario[47]. The SSP 5-8.5 is assumed to represent a high level of urban expansion throughout the twenty-first century. We initially define the urban regions using the urban boundaries provided by the GUB dataset and create the corresponding rural buffers as done in the city-scale analyses. Further, we

https://doi.org/10.1038/s44284-024-00102-z

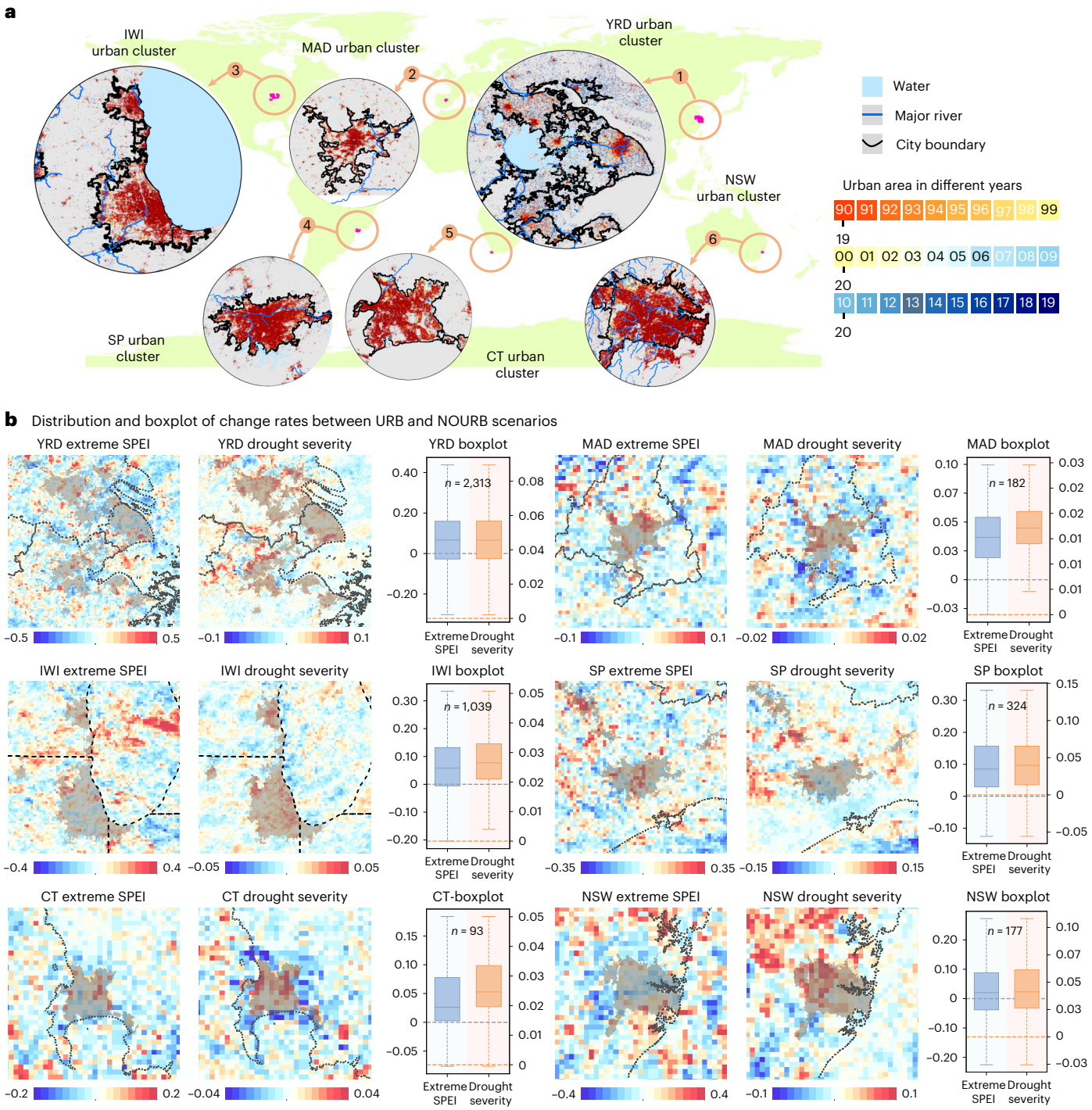


**Fig. 2 | Percentage changes of extreme SPEI and drought severity due to urbanization based on WRF simulation.** To deepen the understanding of urbanization effects on local drought development, we perform WRF simulations over six selected urban clusters across each continent, namely the YRD urban cluster in Asia, the Madrid (MAD) urban cluster in Europe, the IWI urban cluster in North America, the São Paulo urban cluster (SP) in South America, the Cape Town urban cluster (CT) in Africa and the NSW urban cluster in Australia. **a**, Locations and urban development for the six selected regions. **b**, The spatial distributions and box plots of change rates for extreme SPEI and drought severity in each region. Change rates are defined as the relative change of the drought metric in the URB scenario compared to that in the NOURB scenario. A positive change indicates that the drought metric is exacerbated due to urbanization. Gray backgrounds are the major urban regions and dashed lines indicate state and/or provincial boundaries. The change rates in the box plots correspond to drought metrics computed within gray background areas. For each box plot, the center and lower and upper lines of the box represent the median and the 25 and 75% quantiles, respectively. The lower and upper bounds of the whiskers represent minima and maxima with the range based on 1.5× interquartile range.

follow urban expansion estimates from 2020 to 2050 in the SSP 5-8.5 scenario to update our urban or rural classification[48]. Updates of urban and rural regions are conducted for each decade during 2020–2050. After regridding the HighResMIP simulations to 0.1°, we calculate and average the drought metric time series for the updated urban and rural regions and compute the trends for 30 IPCC-AR6 regions.

Figure 4 displays the variations and trends of monthly SPEI based on the ensemble mean of the selected HighResMIP models (Supplementary

https://doi.org/10.1038/s44284-024-00102-z

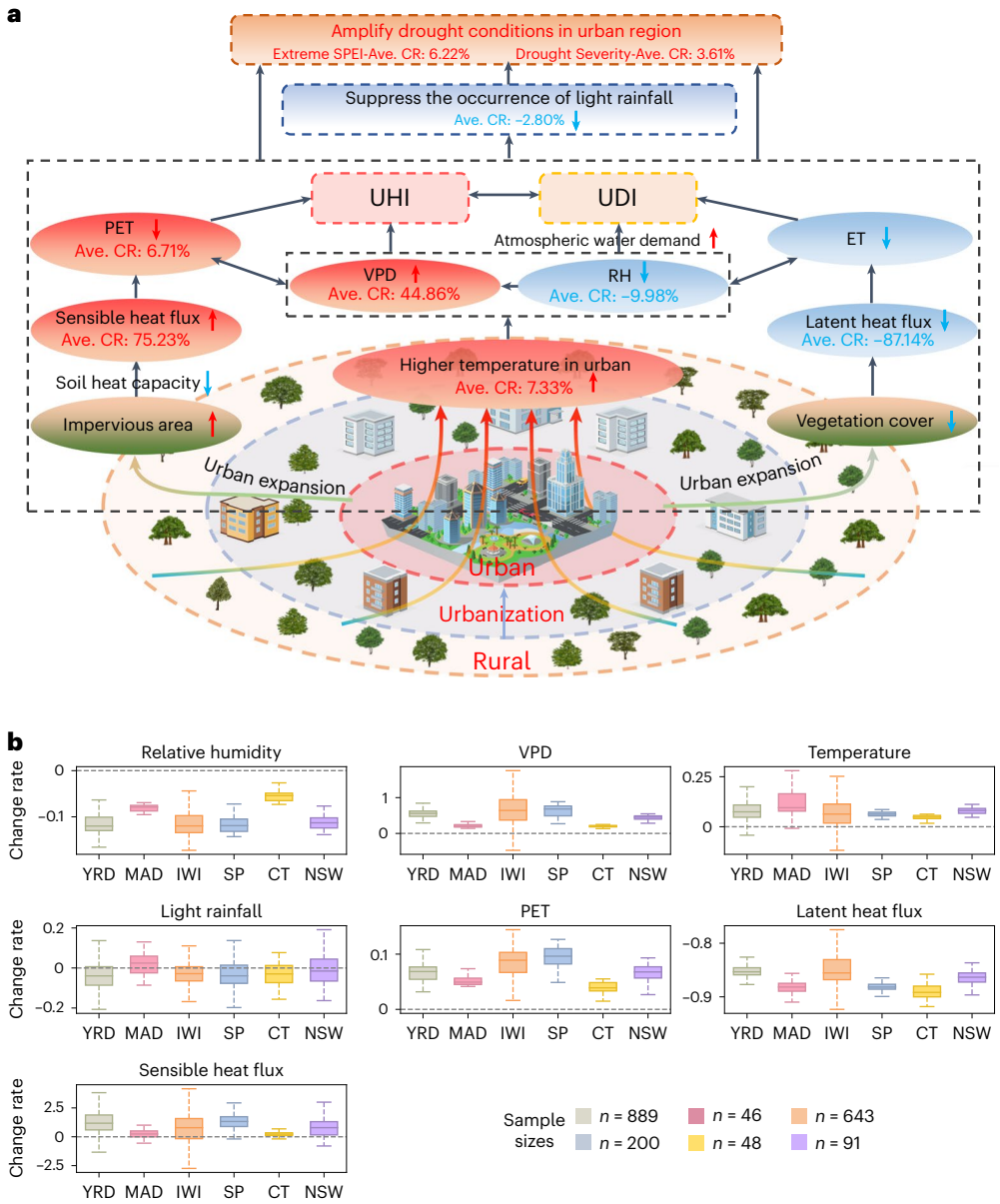


**Fig. 3 | Schematic diagram of potential mechanisms underlying the effects of urbanization on local drought. a**, The potential mechanism of how urbanization affects drought through meteorological and anthropogenic feedbacks. The up and down arrows indicate increase and decrease in a variable due to urbanization. The average change rate (Ave. CR) of each variable over the six regions is also presented in the figure. The tree and building components in **a** are designed by vectorpocket and/or macrovector (Freepik.com). ET, evapotranspiration. **b**, The box plots of the change rates for the WRF-simulated variables in the six regions, including relative humidity (RH), VPD, temperature, light rainfall, PET, latent heat flux and sensible heat flux. For each box plot, the center and lower and upper lines of the box represent the median and the 25 and 75% quantiles, respectively. The lower and upper bounds of the whiskers represent minima and maxima with the range based on 1.5× interquartile range.

Table 2) during the period of 2015 to 2050. Supplementary Fig. 17 shows the results from individual models. In general, the results suggest that drought conditions are expected to be intensified in most regions over the next three decades, as indicated by the overall decreasing trends of the drought metric time series. By comparing trends in the drought metrics between urban and rural grid cells, the effects of urbanization are shown to persist in future scenarios. Among the selected IPCC-AR6 regions, urban SPEI shows a more considerable decrease in 20 out of 30 regions, with an average decreasing slope of −0.0015 per month. Furthermore, Supplementary Figs. 18 and 19 present variations and trends of extreme SPEI and drought severity calculated by daily HighResMIP meteorological data. Results reveal that nearly 70 and 57% of urban regions exhibit worsening extreme SPEI and drought severity, with average slopes of −1.02 and −1.52 $yr^{-1}$, respectively.

Overall, our quantitative results based on historical observational records and our HighResMIP simulation analyses highlight increasing drought with urban expansion, particularly with respect to extreme SPEI and drought severity.

## Discussion

While previous studies have revealed that anthropogenic activities, such as the emission of greenhouse gases, have driven global drought signals throughout the twentieth and twenty-first centuries, the role of urbanization as a notable human contribution to urban hydroclimatic extremes such as droughts has remained uncharacterized[11,32]. Here, we present a comprehensive analysis of the effect of urbanization on local drought using historical evidence and future projections.

https://doi.org/10.1038/s44284-024-00102-z

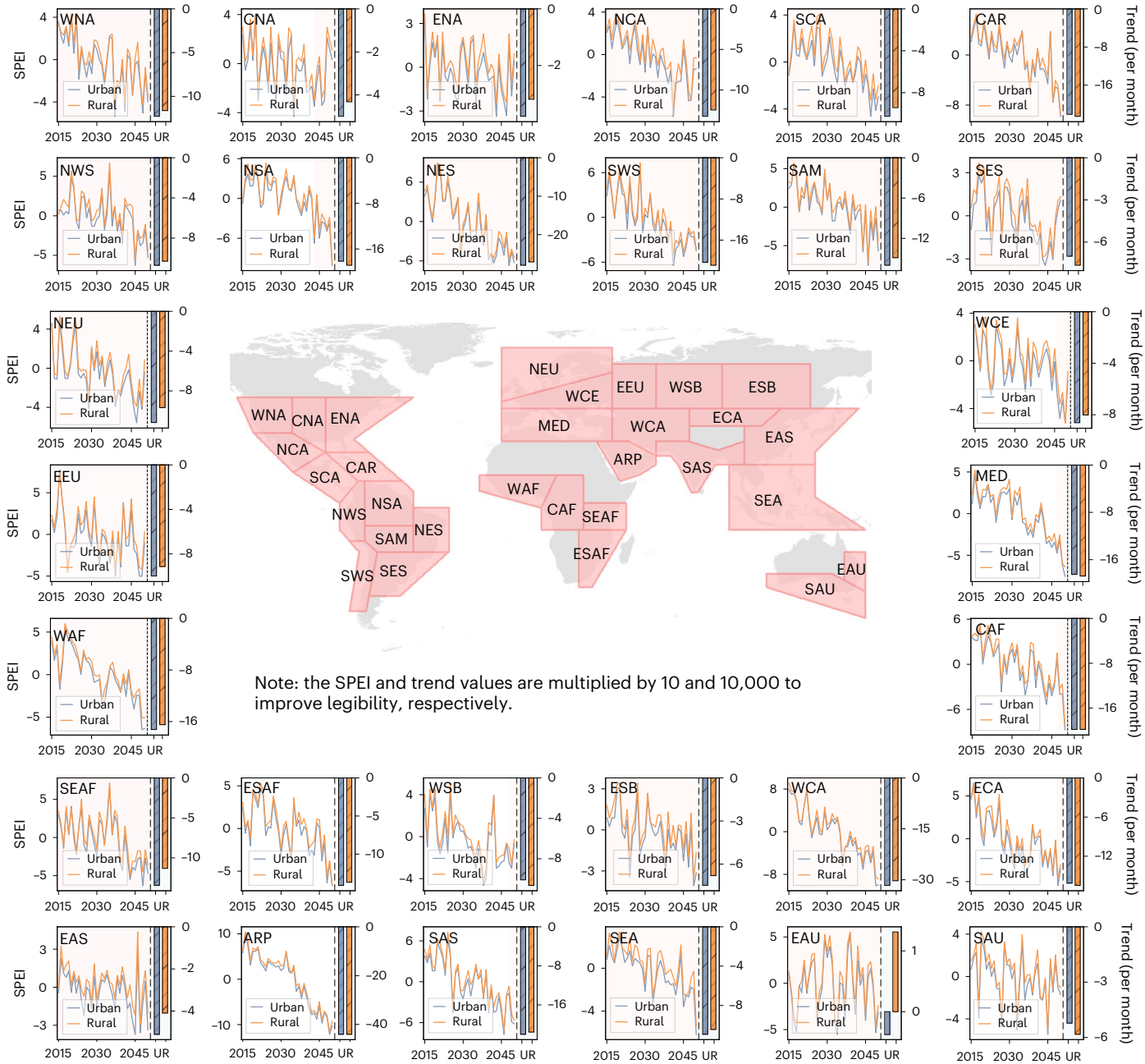


**Fig. 4 | Future projection of urbanization effects on local drought development across different IPCC-AR6 regions based on monthly SPEI.** The central map illustrates the location and extent of each IPCC-AR6 region. For each subfigure, the left axis shows the temporal variations of SPEI in urban (blue line) and rural (orange line) areas, respectively. Here, monthly SPEI is calculated based on the ensemble mean of three HighResMIP models. The bar chart in the right panel represents the trend of the corresponding urban or rural series calculated by Sen's slope. The bar that has passed Mann–Kendall trend test is depicted with diagonal lines. The selected IPCC-AR6 regions include Western North America (WNA), Central North America (CNA), Eastern North America (ENA), Northern Central America (NCA), Southern Central America (SCA), Caribean (CAR), Northwestern South America (NWS), Northern South America (NSA), Northeastern South America (NES), Southwestern South America (SWS), South American Monsoon (SAM), Southeastern South America (SES), Northern Europe (NEU), Western and Central Europe (WCE), Eastern Europe (EEU), Mediterranean (MED), Western Africa (WAF), Central Africa (CAF), South of Eastern Africa (SEAF), East of Southern Africa (ESAF), Western Siberia (WSB), Eastern Siberia (ESB), Western and Central Asia (WCA), Eastern and Central Asia (ECA), Eastern Asia (EAS), Arabian Peninsula (ARP), Southern Asia (SAS), Southeastern Asia (SEA), Eastern Australia (EAU) and Southern Australia (SAU).

From a global perspective, our observational results underscore substantial and non-negligible influences of urbanization on local drought. Over half of the world's cities exhibit pronounced urbanization effects, albeit with discernible disparities in the impacts across different gradations of drought events. In contrast to medium to low intensity level droughts, extreme drought exhibits more significant effects under urbanization, with an overwhelming number of cities exhibiting exacerbated extreme SPEI and drought severity (Fig. 1a,b). The cities that show reduction in drought under urbanization are sparsely scattered across continents but cluster near the coastlines, especially in the western United States and Mediterranean regions[8,49]. Coastal cities benefit from the ocean's moisture source, while land–sea breezes serve to regulate urban sensible heat and elevate humidity levels[50]. For instance, Mediterranean climate leads to lower summer

temperature in coastal cities compared to their inland counterparts, while the influence of the Pacific Ocean helps to moderate wet and dry conditions of the cities in the southwestern US cities (for example, Los Angeles)[49]. These moderating factors, along with mitigated UHI and UDI effects, may partially explain the reduced exacerbation effects of urbanization on local drought potential among coastal cities.

To gain deeper insights into the mechanistic understanding underlying the exacerbation effects of urbanization on local drought, we perform WRF simulations to model the urbanization-induced rainfall changes between a URB and a NOURB in six representative urban regions. Our findings indicate that the transition from rural to highly urbanized setting leads to a roughly 3–9% amplification of extreme SPEI and drought severity. By examining the variations in key drought-related factors between URB and NOURB scenarios, the simulations show that the increased water demand along with the drier and warmer urban environments together contribute to the amplification of drought in urban cores[32,41]. Our simulated results agree with ref. 36, who observed significant surface warming trends in the urban cores relative to rural surroundings in more than 2,000 global cities. The combined effects of UHI and UDI lead to lower probability of the occurrence of light rainfall. Previous studies support our findings that urbanization may enhance the asymmetrical changes in rainfall patterns, where extreme heavy rainfall increases while light rainfall decreases[51]. Nevertheless, it should be noted that the mechanistic pathway that we highlight (Fig. 3) represents just one potential mechanism of the effects of urbanization on local drought, and underlying processes may vary across cities depending on the climatic conditions, vegetation cover, topography and other factors[27]. The complex interaction and feedback between urbanization and land–atmosphere conditions in shaping drought patterns warrant further in-depth and physics-based local studies.

Furthermore, we project the effects of future urbanization on local drought using CMIP6 HighResMIP model simulations. The mid-twenty-first century projection shows that urban regions suffer higher drought risk than rural regions in ~70% of the selected IPCC-AR6 subregions. Amplification of extreme SPEI and drought severity is mainly associated with the conversion of cropland or contemporary vegetated areas into impervious surfaces, resulting in increased sensible heat and reduced atmospheric humidity. Previous research has projected that by 2050, nearly half of the global population living in cities will experience water scarcity[52]. The projected intensification of local drought is likely to aggravate such water-scarce conditions in urban settings. Meanwhile, the projected changes in urban drought will also hinder the realization of at least three Sustainable Development Goals of the UN 2030 Agenda, such as Goal 6 'Clean water and sanitation', Goal 11 'Sustainable cities and communities' and Goal 15 'Life on land'[29].

To cope with the challenge of urban drought, we highlight several nature-based and infrastructure-based actions to help city stakeholders improve urban drought resilience. From a nature-based perspective, urban green spaces (for example, parks, green roofs, wetlands) can in some instances serve as effective mitigators of the effects of urbanization on local drought[36]. Reference 26 analyzed the relationship between urban dryness and evapotranspiration and highlighted the efficiency of restoring evapotranspiration in dealing with the negative effects of the UHI and UDI. In this study, we also observe the reduced urbanization-induced exacerbation effects on local drought with the increased density of vegetation cover (Supplementary Fig. 7). Thus, it is worthy to carefully design, manage and maintain urban vegetation and ecosystems, which are the major regulators of atmospheric moisture in urban areas[53]. From an anthropogenic infrastructure-based perspective, a more flexible and reliable urban water supply system is needed. For instance, the urban water supply portfolio should be diversified by considering various alternative water sources, including desalination, sectional water transfer, urban rainwater harvesting and greywater recycling[28,52]. In addition to nature-based and infrastructure-based solutions, development of comprehensive water management plans that include public awareness education and water conservation measures are needed[29].

We acknowledge the presence of several limitations in our study. Previous research has confirmed the uncertainties of CMIP6 models in the projection of anthropogenic effects[6,54]. Similarly, biases also appear in the WRF simulations, influenced by the initial and boundary conditions and parameterization[55]. Consequently, the quantitative results may exhibit a degree of error. Nevertheless, given our study's emphasis on discerning differences between urban–rural pairs and model experiments, the inherent biases are minimized[6]. In addition, we recognize that while long-term drought events can inflict lasting damage on urban ecosystems, we define drought on a short-term daily scale to facilitate a more precise quantification of different drought levels and to capture the immediate impacts of urbanization, which are particularly relevant in light of the increasing frequency of flash droughts[3,27,56]. We also perform sensitivity tests by using monthly scale SPEI and the results generally align with the evidence based on daily data. Moreover, constrained by the lack of globally applicable long-term and high-resolution (both spatial and temporal) meteorological satellite data for urban areas, we mainly adopt in situ observations, ERA5-Land product and CMIP6 simulations with barely satisfactory spatial resolution (~10–25 km). Likewise, the future projection is only conducted in SSP 5-8.5 scenario due to the lack of lower emission scenarios data with relatively high spatial resolution. In future work, it would be ideal to work with higher spatial resolution fusion datasets and model simulations (for example, SSP 1-2.6, SSP 2-4.5, SSP 3-7.0) to deepen our understanding of local drought changes and its evolutions. It is also important to note that, drought is not only deficit in rainfall and the SPEI or changes in rainfall relative to urbanization. Demand, which is an important component, is not considered in this study, especially for the future projections.

By providing these insights into the drought responses to urbanization, our quantitative results highlight the uneven contribution of urbanization on local drought. Again, these results are not inconsistent to the rainfall enhancement noted due to urbanization in prior studies. This is because, the enhancement over or downwind of cities also implies reduction in the vicinity of cities. From the perspectives of observation to model simulation and historical evidence to future projection, we confirm the overwhelming exacerbation of extreme SPEI and drought severity under urbanization and explore the potential mechanism. As urban expansion continues alongside population growth, cities are confronted with substantial challenges in reconciling increased water demand with diminished water supply under global warming and drought stress. In pursuit of sustainable urban development, our findings seek to add further body of evidence and implications on the role of urbanization in driving local drought variations and hydroclimatic extremes.

## Methods

### Data

**In situ data.** We collected observational daily precipitation and temperature data from multiple sources, including the Global Surface Summary of the Day (GSOD), Global Historical Climatology Network (GHCN), European Climate Assessment Dataset (ECAD) and the China Meteorological Administration (CMA), spanning the period from 1980 to 2020 (refs. 32,57). Our initial step involved the removal of duplicate stations from these four datasets. Subsequently, we conducted a quality control process to eliminate low-quality and missing data points based on quality control files. Specifically, for GHCN data, the records with an observation value of 9,999 (that is, missing data) and quality flag other than blank (that is, did not fail any quality assurance check) were removed. For GSOD, the records with observation values of 99.99 or 9,999.9 and quality attributes of incomplete data reports were removed. For ECAD, the records with quality code of '1' (that is,

suspect) and '9' (that is, missing) were removed. For CMA, the records with observation values of 32,766 (that is, missing) and quality code other than '0' were removed. To ensure adequate quantity of observations, we retained only the sites with over 75% completeness for both precipitation and temperature records. To fill the gap of the missing values for each station, we adopted three multi-source meteorological products, including Climate Hazards Group InfraRed Precipitation with Station data (CHIRPS), NOAA Climate Prediction Centre (CPC) and ERA5-Land[58,59]. The selections of these three products were based on the sufficient time range (1980–2020) and relatively high spatio-temporal resolution compared to the available precipitation products (Supplementary Table 1). Due to the scale mismatch between station-scale (point) data and gridded data (pixel), errors may exist between the in situ measurements and these three products. To minimize the uncertainties of the individual products, the ensemble mean of these three products was calculated to fill the missing values. Finally, the spatial distribution of the processed stations is shown in Supplementary Fig. 1a.

**Model-based data.** To study the urbanization effects on the city scale, we used the hourly fifth-generation European Centre for Medium-Range Weather Forecasts atmospheric reanalysis of the global climate (ERA5-Land) with 0.1° spatial resolution during the period of 1980 to 2020 (ref. 59). The selected variables included total precipitation, 2 m temperature, dewpoint temperature, wind speed, surface solar radiation downwards and surface pressure. The hourly data were resampled to daily data. Meanwhile, we also used ERA5 at all pressure levels and surface level as the initial and boundary conditions for WRF simulation.

CMIP6 was applied in our study for future projection[60]. Specifically, to project the future changes of local drought under urbanization, we used monthly and daily HighResMIP models in CMIP6. In this case, we only used the precipitation and temperature data because of the limited availability of high-resolution meteorological variables in the HighResMIP mode. Supplementary Table 2 lists the selected HighResMIP models for future projection of urbanization effects.

**Auxiliary data.** For the classification of urban and rural regions, we first obtained Global Impervious Surface Area 2.0 (GISA2.0) product with a spatial resolution of 30 m. The GISA2.0 has improved from its predecessor by dividing the grid and performing with different enhancement techniques, which has shown excellent performance in urban studies[61]. We also adopted GUB data, which can capture the geolocations of world's cities well[33]. The land cover data were obtained from yearly MCD12Q1 product, which follows the International Geosphere-Biosphere Programme classification system. We also adopted the future urban expansion data from 2020 to 2050 under the SSP 5-8.5 scenario generated by ref. 48. In addition, the 1 km Köppen–Geiger climate classification data were used to define the major climate zones for the investigation of urbanization effects under different climatic backgrounds[62].

## Definition of drought metrics

To examine the urbanization effects on local meteorological drought, we took the Standardized Precipitation Evapotranspiration Index (SPEI) as the major index to characterize drought condition[63]. Superior to drought indices such as Palmer Drought Severity Index, SPEI has flexible timescale, which enables it to monitor short-, mid- and long-term drought conditions. Meanwhile, as urbanization usually accompanies with frequent alteration of impervious surface and vegetation cover, the consideration of evapotranspiration in SPEI can make it better reflect the impact of atmospheric dryness on water resources and ecosystems.

SPEI is obtained by normalizing the water balance (calculated by precipitation minus PET) into log-logistic distribution, which was widely adopted in previous studies[6,64]. There are various methods to calculate PET, including the widely used Thornthwaite method and the acknowledged most accurate FAO-56 Penman–Monteith method. Considering the limited number of variables provided by in situ stations, we adopted Thornthwaite method to calculate PET for observational data. The equation of Thornthwaite method is given as follows:

$$\mathrm{PET} = \begin{cases} 16C\left(\frac{10T}{I}\right)^{a} & 0 \le T \le 26.5\,^{\circ}\mathrm{C} \\ C\left(-415.85 + 32.24T - 0.43T^{2}\right) & T > 26.5\,^{\circ}\mathrm{C} \end{cases} \quad (1)$$

where $T$ and $I$ are temperature and thermal index, respectively, and $a$ is a function of $I$. The detailed calculation can refer to ref. 65. In addition, to compare with the Thornthwaite-based results, we also applied Penman–Monteith equation to calculate PET in city-scale analysis as ERA5-Land could provide sufficient number of variables. The Penman–Monteith equation is given as follows:

$$\mathrm{PET} = \frac{0.408\Delta\,(R_{\mathrm{n}} - G) + \gamma\frac{900}{(T+273)}u_2(e_{\mathrm{s}} - e_{\mathrm{a}})}{\Delta + \gamma(1 + 0.34u_2)} \quad (2)$$

where $T$ and $u_2$ are daily air temperature and 2 m wind speed; $\Delta$ is the slope of vapor pressure curve; $R_{\mathrm{n}}$ is the net radiation; $G$ is the soil heat flux density; $e_{\mathrm{s}}$ and $e_{\mathrm{a}}$ are the saturation vapor pressure and actual vapor pressure, respectively, and $\gamma$ is the air psychrometric constant[66]. Here we also evaluate the performance of PET calculated by Thornthwaite and Penman–Monteith methods for all in situ stations in 2020 (Supplementary Fig. 2). Although differences exist between the Thornthwaite PET and Penman–Monteith PET, the results show a significant positive relationship with Pearson correlation coefficient, root mean square error (r.m.s.e.) and mean absolute error of 0.843, 1.013 mm and 0.913 mm, respectively. In other words, the Thornthwaite PET is able to present similar trend as Penman–Monteith PET.

To further characterize drought development in urban regions, we defined six drought metrics based on SPEI[32]. First, for each single unit (that is, station or pixel), we determined the thresholds for extreme, heavy, moderate and light SPEI as the 5th, 10th, 20th and 30th percentiles of the SPEI during the period of 1980 to 2000 (ref. 67). Then the extreme, heavy, moderate and light SPEI values were classified on the basis of the defined thresholds and the annual sums for extreme, heavy, moderate and light SPEI were calculated for each year, respectively. In addition, we extracted two major drought characteristics (that is, drought duration and drought severity) based on run theory. The run theory can identify drought events based on SPEI series (Supplementary Fig. 3). For each drought event, the drought duration is the time length of the event and the drought severity is the cumulative negative SPEI values during the drought event. The annual total duration and severity were further calculated based on the identified drought events in each year.

## Quantification of urbanization effects on local drought

To quantify the effects of urbanization on local drought, we first classify urban and rural stations by considering the dynamic land use changes, using the time-varying GISA2.0 data[44]. The study period (1980–2020) was separated at intervals of 5 years. In each subperiod, a circular buffer was created for every station and the proportion of impervious surface area within the buffer was calculated. A station was defined as an urban station only if the impervious fraction exceeded a predefined threshold. Otherwise, the station was determined to be a rural station. In this case, each station was dynamically classified as urban or rural during 1980–2020. Here the buffer radius and impervious surface threshold were determined by calculating the correlation coefficient between meteorological series and urban expansion rate for buffers with different buffer sizes[51,68,69]. Following previous studies[10,14,32,51], typical selections of buffer radius (km) and impervious surface threshold (%) include 7 km and 20% and 2 km and 33%. The former combination

is usually applied when using 1 km of LULC (land use land cover) data to classify urban and rural stations, while 2 km and 33% is the most frequently chosen when using 30 m LULC data. Considering the use of 30 m impervious surface area data in this study, we finally selected 2 km and 33% as the buffer radius and impervious surface threshold to classify urban and rural stations.

To reduce the impacts of potential regional confounding factors, for each urban station, we paired its rural stations within its 100 km buffer zone[68,70]. The rural stations with elevation difference larger than 500 m from paired urban station were further excluded to minimize the topographical effects. For each urban–rural pair, the urban and rural mean drought series were then calculated by averaging all urban and rural stations within the pair based on the dynamic station classification results. It should be noted that if the urban station in an urban–rural pair was classified as the rural station in the early period according to the dynamic classification, its drought series in this period was replaced as the average of all rural stations within the pair. Then the differences of drought metrics between the urban and rural stations within an urban–rural pair were assumed as the contribution of urbanization[50,68,70].

After the classification and pairing of urban and rural stations, we quantified the urbanization effects (UE) by Mann–Kendall trend test and Sen's slope. The urbanization effect can be quantified as follows[45,51]:

$$\mathrm{UE} = T_{\mathrm{urban}} - T_{\mathrm{rural}} \tag{3}$$

where $T_{\mathrm{urban}}$ and $T_{\mathrm{rural}}$ are the Sen's slope of average urban and rural drought series of an urban–rural pair, respectively. The negative (positive) value of UE represents a negative (positive) urbanization effect, indicating exacerbation (mitigation) effect on local drought. The significance (95% confidence level) of the urbanization effect can be examined by calculating the Mann–Kendall trend of the differences between urban and rural series.

In addition to the station-scale analysis, we also investigated the effects of urbanization on local drought by using GUB data to classify the areal urban and rural regions (that is, city-scale analysis). To ensure available pixels for further calculation, we removed city boundaries with areas smaller than 100 km$^2$ and a total of 1,029 city boundaries were selected. The locations of selected cities are shown in Supplementary Fig. 1b. Each selected urban boundary was regarded as the urban region. To determine the corresponding rural region, for each city boundary, we created a buffer outward with the buffer distance calculated by[34]:

$$D = \left(\sqrt{2} - 1\right)\sqrt{\frac{S}{\pi}} \tag{4}$$

where $S$ represents the area of the city. The function can ensure that the area of urban region is approximately the same as its outward buffer (that is, rural area). The drought metrics for the urban and rural boundaries were calculated based on the ERA5-Land data. Then equation (3) was applied to calculate urbanization effects on the city scale.

Urbanization is also likely to affect the drought frequency. Here we used return period to characterize the drought frequency, which represents the historical interval of a drought event with given duration and severity. To investigate the association between urbanization and drought frequency, we calculated the return period using copula functions. Copula is usually applied to establish the joint probability distribution of multiple variables in the field of drought and flood estimation. In drought-related studies, the copula functions can calculate the return period for joint occurrence of drought characteristics[71]. In this study, we adopted exponential distribution and gamma distribution as the marginal distributions to fit drought severity and drought duration following previous studies[72]. The bivariate Gumbel copula was then used to construct the joint distribution for drought severity and duration. In general, the return period can be classified into two types, namely an AND return period (both the given duration and severity are exceeded) or a OR return period (either the given duration or severity is exceeded), which can be calculated as:

$$T_{\mathrm{AND}} = \frac{E(L)}{1 - F_{\mathrm{D}}(d) - F_{\mathrm{S}}(s) + C\left(F_{\mathrm{D}}(d), F_{\mathrm{S}}(s)\right)} \quad (D \geq d \text{ AND } S \geq s) \tag{5}$$

$$T_{\mathrm{OR}} = \frac{E(L)}{1 - C\left(F_{\mathrm{D}}(d), F_{\mathrm{S}}(s)\right)} \quad (D \geq d \text{ OR } S \geq s) \tag{6}$$

where $D$ and $S$ are drought duration and severity; $L$ is the interval between the onset of two adjacent drought events while $E(L)$ is the average of $L$; $F_{\mathrm{D}}$ and $F_{\mathrm{S}}$ are the marginal distributions of drought duration and severity, and $C$ is the joint copula function. The difference of return period between paired urban and rural series was regarded as the urbanization effect on drought frequency.

### WRF simulations for potential mechanism analysis

We used WRF coupled with single-layer urban canopy model to simulate the drought development across typical urban clusters. We selected a total of six representative urban clusters that had suffered severe drought across different climatic backgrounds and continents, including the YRD urban cluster in Asia, Madrid urban cluster in Europe, IWI urban cluster in North America, São Paulo (SP) urban cluster in South America, Cape Town urban cluster in Africa and NSW urban cluster in Australia. The model was configured to have 9–3 km nested domain. We ran the WRF simulation during the historical drought years for each urban region (2010–2012 for YRD, 2013–2015 for the Madrid urban cluster, 2011–2013 for IWI, 2013–2015 for SP, 2015–2017 for Cape Town, 2017–2019 for NSW). The first month for each year was set as the spin-up period. The detailed information of each domain is shown in Supplementary Table 3. The model configuration is listed in Supplementary Table 4. To validate the performance of WRF simulations, we selected the middle year of simulation periods in the URB scenario (which used the actual LULC data) for each region (that is, 2011 for YRD, 2014 for the Madrid urban cluster, 2012 for IWI, 2014 for SP, 2016 for Cape Town, 2018 for NSW) as the validation period. The simulated precipitation and temperature were validated against local in situ measurements. For each region, the average observed and WRF-simulated precipitation and/or temperature are calculated over all validation stations and their corresponding model grid cells, respectively. The Pearson correlation coefficient, r.m.s.e. and mean absolute error were used to evaluate the simulation performance.

To evaluate urbanization effects on local drought development in urban regions, we designed two separate experiments with different input LULC data for each region. The highly URB used the normal LULC data of the simulation year as the input. We further replaced the urban pixels of the URB LULC data with the other dominant land cover type to simulate a NOURB. The ERA5 with single level and pressure level was used as the initial boundary condition. The first month of the simulation period was regarded as the spin-up period. To validate performance of the model simulation, we compared the simulated precipitation and temperature with the in situ measurements obtained from the weather stations near the cities. Finally, by comparing the differences of drought development in URB and NOURB cases, we were able to investigate the urbanization effects on drought in local scale.

### Reporting summary

Further information on research design is available in the Nature Portfolio Reporting Summary linked to this article.

## Data availability

GSOD and GHCN global in situ meteorological data can be accessed at https://www.ncei.noaa.gov/data/global-summary-of-the-day/ and

https://www.ncei.noaa.gov/data/global-historical-climatology-network-daily/. CMA meteorological data are available at http://data.cma.cn/en/?r=data/detail&dataCode=A.0012.0001. ECAD data are available at https://www.ecad.eu/dailydata/predefinedseries.php. ERA5-Land and ERA5 products are obtained from https://cds.climate.copernicus.eu/cdsapp#!/dataset/reanalysis-era5-land?tab=form and https://cds.climate.copernicus.eu/cdsapp#!/dataset/reanalysis-era5-pressure-levels?tab=form. CHIRPS precipitation can be retrieved at https://data.chc.ucsb.edu/products/CHIRPS-2.0/. CRU product is available at https://crudata.uea.ac.uk/cru/data/hrg/cru_ts_4.06/. CPC data can be accessed at https://downloads.psl.noaa.gov/Datasets/cpc_global_precip/. CMIP6 simulation data are obtained from https://esgf-node.llnl.gov/search/cmip6/. The GISA2.0 product is available via Zenodo at https://zenodo.org/record/6476661 (ref. 73). GUB data can be obtained at http://data.starcloud.pcl.ac.cn/zh/resource/14. Koppen climate classification product is provided by https://www.gloh2o.org/koppen. MCD12Q1 product is provided by https://e4ftl01.cr.usgs.gov/MOTA/MCD12Q1.061/. The future urban expansion data are available at https://doi.org/10.1594/PANGAEA.905890. All base maps used in this study are obtained from the Database of Global Administrative Areas (GADM) at https://gadm.org/download_world.html.

## Code availability

The data analysis was conducted using Python v.9, MATLAB v.022b and ArcMap v.0.6. The code and necessary data can be accessed on GitHub (https://github.com/szhuangGIS/Urbanization-Drought). Additional code and data related to this paper are available from the corresponding authors upon reasonable request.

## References


1. Sternberg, T. Regional drought has a global impact. *Nature* **472**, 169 (2011).
2. Kreibich, H. et al. The challenge of unprecedented floods and droughts in risk management. *Nature* **608**, 80–86 (2022).
3. Yuan, X. et al. A global transition to flash droughts under climate change. *Science* **380**, 187–191 (2023).
4. Spinoni, J., Naumann, G., Carrao, H., Barbosa, P. & Vogt, J. World drought frequency, duration, and severity for 1951-2010. *Int. J. Climatol.* **34**, 2792–2804 (2014).
5. Rodell, M. & Li, B. Changing intensity of hydroclimatic extreme events revealed by GRACE and GRACE-FO. *Nat. Water* **1**, 241–248 (2023).
6. Chiang, F., Mazdiyasni, O. & AghaKouchak, A. Evidence of anthropogenic impacts on global drought frequency, duration, and intensity. *Nat. Commun.* **12**, 2754 (2021).
7. Chai, R. et al. Human-caused long-term changes in global aridity. *npj Clim. Atmos. Sci.* **4**, 65 (2021).
8. Li, L. et al. Divergent urbanization-induced impacts on global surface urban heat island trends since 1980s. *Remote Sens. Environ.* **295**, 113650 (2023).
9. Ouyang, Z. et al. Albedo changes caused by future urbanization contribute to global warming. *Nat. Commun.* **13**, 3800 (2022).
10. Sun, Y., Zhang, X., Ren, G., Zwiers, F. W. & Hu, T. Contribution of urbanization to warming in China. *Nat. Clim. Change* **6**, 706–709 (2016).
11. AghaKouchak, A. et al. Anthropogenic drought: definition, challenges, and opportunities. *Rev. Geophys.* **59**, e2019RG000683 (2021).
12. Van Loon, A. F. et al. Drought in the Anthropocene. *Nat. Geosci.* **9**, 89–91 (2016).
13. Freitag, B., Nair, U. & Niyogi, D. Urban modification of convection and rainfall in complex terrain. *Geophys. Res. Lett.* **45**, 2507–2515 (2018).
14. Wang, J. et al. Anthropogenic emissions and urbanization increase risk of compound hot extremes in cities. *Nat. Clim. Change* **11**, 1084–1089 (2021).
15. Guerreiro, S. B. et al. Detection of continental-scale intensification of hourly rainfall extremes. *Nat. Clim. Change* **8**, 803–807 (2018).
16. Zhang, K. et al. Increased heat risk in wet climate induced by urban humid heat. *Nature* **617**, 738–742 (2023).
17. Massaro, E. et al. Spatially-optimized urban greening for reduction of population exposure to land surface temperature extremes. *Nat. Commun.* **14**, 2903 (2023).
18. Yang, L. et al. Urban development pattern's influence on extreme rainfall occurrences. *Nat. Commun.* **15**, 3997 (2024).
19. Liu, J. & Niyogi, D. Meta-analysis of urbanization impact on rainfall modification. *Sci. Rep.* **9**, 7301 (2019).
20. Singh, J. et al. Urbanization alters rainfall extremes over the contiguous United States. *Environ. Res. Lett.* **15**, 074033 (2020).
21. Shepherd, J. M. & Burian, S. J. Detection of urban-induced rainfall anomalies in a major coastal city. *Earth Interact.* **7**, 1–17 (2003).
22. Shepherd, J. M. A review of current investigations of urban-induced rainfall and recommendations for the future. *Earth Interact.* **9**, 1–27 (2005).
23. Yang, L., Ni, G., Tian, F. & Niyogi, D. Urbanization exacerbated rainfall over European suburbs under a warming climate. *Geophys. Res. Lett.* **48**, e2021GL095987 (2021).
24. Huang, X. et al. Urbanization aggravates effects of global warming on local atmospheric drying. *Geophys. Res. Lett.* **49**, e2021GL095709 (2022).
25. *World Urbanization Prospects: The 2018 Revision* (United Nations, 2018); www.un.org/en/desa/2018-revision-world-urbanization-prospects
26. Hao, L. et al. Urbanization alters atmospheric dryness through land evapotranspiration. *npj Clim. Atmos. Sci.* **6**, 149 (2023).
27. Ghanbari, M., Arabi, M., Georgescu, M. & Broadbent, A. M. The role of climate change and urban development on compound dry-hot extremes across US cities. *Nat. Commun.* **14**, 3509 (2023).
28. Cremades, R. et al. Guiding cities under increased droughts: the limits to sustainable urban futures. *Ecol. Econ.* **189**, 107140 (2021).
29. Zhang, X. et al. Urban drought challenge to 2030 sustainable development goals. *Sci. Total Environ.* **693**, 133536 (2019).
30. Millington, N. Producing water scarcity in São Paulo, Brazil: the 2014–2015 water crisis and the binding politics of infrastructure. *Polit. Geogr.* **65**, 26–34 (2018).
31. Rusca, M., Savelli, E., Di Baldassarre, G., Biza, A. & Messori, G. Unprecedented droughts are expected to exacerbate urban inequalities in Southern Africa. *Nat. Clim. Change* **13**, 98–105 (2022).
32. Huang, S. et al. Urbanization amplified asymmetrical changes of rainfall and exacerbated drought: analysis over five urban agglomerations in the Yangtze River Basin, China. *Earth's Future* **11**, e2022EF003117 (2023).
33. Li, X. et al. Mapping global urban boundaries from the global artificial impervious area (GAIA) data. *Environ. Res. Lett.* **15**, 094044 (2020).
34. Zhang, L. et al. Direct and indirect impacts of urbanization on vegetation growth across the world's cities. *Sci. Adv.* **8**, eabo0095 (2022).
35. Hao, L. et al. Ecohydrological processes explain urban dry island effects in a wet region, Southern China. *Water Resour. Res.* **54**, 6757–6771 (2018).
36. Liu, Z. et al. Surface warming in global cities is substantially more rapid than in rural background areas. *Commun. Earth Environ.* **3**, 219 (2022).
37. Leeper, R. D. et al. Characterizing U.S. drought over the past 20 years using the U.S. drought monitor. *Int. J. Climatol.* **42**, 6616–6630 (2022).
38. Moravec, V. et al. Europe under multi-year droughts: how severe was the 2014–2018 drought period? *Environ. Res. Lett.* **16**, 034062 (2021).

39. Tian, F. et al. Exceptional drought across southeastern Australia caused by extreme lack of precipitation and its impacts on NDVI and SIF in 2018. *Remote Sensing* **12**, 54 (2019).
40. Li, W. et al. Widespread and complex drought effects on vegetation physiology inferred from space. *Nat. Commun.* **14**, 4640 (2023).
41. Brunsell, N. A., Jones, A. R., Jackson, T. L. & Feddema, J. J. Seasonal trends in air temperature and precipitation in IPCC AR4 GCM output for Kansas, USA: evaluation and implications. *Int. J. Climatol.* **30**, 1178–1193 (2009).
42. Wever, N. Quantifying trends in surface roughness and the effect on surface wind speed observations. *J. Geophys. Res. Atmos.* **117**, D11104 (2012).
43. Peng, S. S. et al. Afforestation in China cools local land surface temperature. *Proc. Natl Acad. Sci. USA* **111**, 2915–2919 (2014).
44. Huang, S. et al. Urbanization-induced drought modification: example over the Yangtze River Basin, China. *Urban Climate* **44**, 101231 (2022).
45. Luo, M. & Lau, N. C. Urban expansion and drying climate in an urban agglomeration of East China. *Geophys. Res. Lett.* **46**, 6868–6877 (2019).
46. Meili, N., Paschalis, A., Manoli, G. & Fatichi, S. Diurnal and seasonal patterns of global urban dry islands. *Environ. Res. Lett.* **17**, 054044 (2022).
47. Haarsma, R. J. et al. High resolution model intercomparison project (HighResMIP v1.0) for CMIP6. *Geosci. Model Dev.* **9**, 4185–4208 (2016).
48. Chen, G. et al. Global projections of future urban land expansion under Shared Socioeconomic Pathways. *Nat. Commun.* **11**, 537 (2020).
49. Tan, X. et al. Increasing global precipitation whiplash due to anthropogenic greenhouse gas emissions. *Nat. Commun.* **14**, 2796 (2023).
50. Zhou, X. et al. Evaluation of urban heat islands using local climate zones and the influence of sea-land breeze. *Sustain Cities Soc* **55**, 102060 (2020).
51. Yu, X. et al. Asymmetrical shift toward less light and more heavy precipitation in an urban agglomeration of East China: intensification by urbanization. *Geophys. Res. Lett.* **49**, e2021GL097046 (2022).
52. He, C. et al. Future global urban water scarcity and potential solutions. *Nat. Commun.* **12**, 4667 (2021).
53. Cuthbert, M. O., Rau, G. C., Ekström, M., O'Carroll, D. M. & Bates, A. J. Global climate-driven trade-offs between the water retention and cooling benefits of urban greening. *Nat. Commun.* **13**, 518 (2022).
54. Zhu, Y., Zhang, R.-H. & Sun, J. North Pacific Upper-Ocean cold temperature biases in CMIP6 simulations and the role of regional vertical mixing. *J. Clim.* **33**, 7523–7538 (2020).
55. Wang, J., Feng, J. & Yan, Z. Potential sensitivity of warm season precipitation to urbanization extents: modeling study in Beijing-Tianjin-Hebei urban agglomeration in China. *J Geophys Res Atmos* **120**, 9408–9425 (2015).
56. Tyagi, S. et al. Flash drought: review of concept, prediction and the potential for machine learning, deep learning methods. *Earth's Future* **10**, e2022EF002723 (2022).
57. Menne, M. J., Durre, I., Vose, R. S., Gleason, B. E. & Houston, T. G. An overview of the Global Historical Climatology Network-Daily Database. *J. Atmos. Oceanic Technol.* **29**, 897–910 (2012).
58. Funk, C. et al. The climate hazards infrared precipitation with stations—a new environmental record for monitoring extremes. *Sci. Data* **2**, 150066 (2015).
59. Muñoz-Sabater, J. et al. ERA5-Land: a state-of-the-art global reanalysis dataset for land applications. *Earth Syst. Sci. Data* **13**, 4349–4383 (2021).
60. Eyring, V. et al. Overview of the Coupled Model Intercomparison Project Phase 6 (CMIP6) experimental design and organization. *Geosci. Model Dev.* **9**, 1937–1958 (2016).
61. Huang, X. et al. Toward accurate mapping of 30-m time-series global impervious surface area (GISA). *Int. J. Appl. Earth Obs. Geoinf.* **109**, 102787 (2022).
62. Beck, H. E. et al. Present and future Köppen-Geiger climate classification maps at 1-km resolution. *Sci. Data* **5**, 180214 (2018).
63. Vicente-Serrano, S. M. et al. Response of vegetation to drought time-scales across global land biomes. *Proc. Natl Acad. Sci. USA* **110**, 52–57 (2012).
64. Zhang, W. et al. Recent decrease of the impact of tropical temperature on the carbon cycle linked to increased precipitation. *Nat. Commun.* **14**, 965 (2023).
65. Pereira, A. R. & Pruitt, W. O. Adaptation of the Thornthwaite scheme for estimating daily reference evapotranspiration. *Agric. Water Manage.* **66**, 251–257 (2004).
66. Yang, Y. et al. Evaluation of six equations for daily reference evapotranspiration estimating using public weather forecast message for different climate regions across China. *Agric. Water Manage.* **222**, 386–399 (2019).
67. Svoboda, M. et al. The frought monitor. *Bull. Am. Meteorol. Soc.* **83**, 1181–1190 (2002).
68. Ren, G. & Zhou, Y. Urbanization effect on trends of extreme temperature indices of national stations over mainland China, 1961–2008. *J. Clim.* **27**, 2340–2360 (2014).
69. Liao, W. et al. Stronger contributions of urbanization to heat wave trends in wet climates. *Geophys. Res. Lett.* https://doi.org/10.1029/2018GL079679 (2018).
70. Luo, M. & Lau, N. C. Increasing heat stress in urban areas of Eastern China: acceleration by urbanization. *Geophys. Res. Lett.* https://doi.org/10.1029/2018GL080306 (2018).
71. Sadeghfam, S., Mirahmadi, R., Khatibi, R., Mirabbasi, R. & Nadiri, A. A. Investigating meteorological/groundwater droughts by copula to study anthropogenic impacts. *Sci. Rep.* **12**, 8285 (2022).
72. Hao, Z., Hao, F., Singh, V. P., Ouyang, W. & Cheng, H. An integrated package for drought monitoring, prediction and analysis to aid drought modeling and assessment. *Environ. Modelling Softw.* **91**, 199–209 (2017).
73. Huang, X. et al. Toward accurate mapping of 30-m time-series global impervious surface area (GISA 2.0). *Zenodo* https://doi.org/10.5281/zenodo.5136329 (2022).


## Acknowledgements

N.C. acknowledges financial support from the Special Fund of Hubei Luojia Laboratory (grant no. 220100034) and the National Natural Science Foundation of China program (grant nos. 41890822, 41801339). C.W. acknowledges financial support from the National Key Research and Development Program of China (grant no. 2023YFC3209101), the Key R&D Program of Hubei Province (grant no. 2022BAA048), the National Nature Science Foundation of China Program (grant no. 42371101), the CRSRI Open Research Program (Program SN: grant no. CKWV20231198/KY) and the Open Fund of National Engineering Research Center for Geographic Information System, China University of Geosciences, Wuhan 430074, China (grant no. 2022KFJJ07). X.Z. acknowledges financial support from the Open Fund of Hubei Luojia Laboratory (grant no. 220100059) and the Open Fund of Key Laboratory of Hydrometeorological Disaster Mechanism and Warning of Ministry of Water Resources (grant no. HYMED202302). S.W. acknowledges support from the Natural Science Foundation of Hubei Province of China (grant no. 2024AFB061). D.E.H. acknowledges support from the U.S. National Science Foundation PREEVENTS (grant no. 1854951). D. N. acknowledges William Stamps Farish Chair endowment from the Jackson School of Geosciences, University of Texas at Austin, and US National Science Foundation

award #2413827 (Extreme Summer Urban Rainfall Modification under Urban Expansion in a Changing Climate). The numerical calculations in this paper have been done on the supercomputing system in the Supercomputing Center of Wuhan University.

## Author contributions

S.H. contributed to the conceptualization, methodology, formal analysis and writing of the paper. S.W. contributed to the methodology, formal analysis, review and editing of the paper. Y.G. contributed to the WRF simulation experiment. N.C. and C.W. contributed to the conceptualization, funding acquisition, review and editing, supervision, and project administration of the paper. X.Z. contributed to the conceptualization and review of the paper. D.N. contributed to the conceptualization, review and editing of the paper. D.E.H., C.L., and J.X. contributed to the review and editing of the paper.

## Competing interests

The authors declare no competing interests.

## Additional information

**Supplementary information** The online version contains supplementary material available at https://doi.org/10.1038/s44284-024-00102-z.

**Correspondence and requests for materials** should be addressed to Chao Wang or Nengcheng Chen.

**Peer review information** *Nature Cities* thanks Akintomide Akinsanola, Gloria Soto Montes de Oca and the other, anonymous, reviewer(s) for their contribution to the peer review of this work.

nature portfolio

Corresponding author(s): Nengcheng Chen, Chao Wang

Last updated by author(s): Mar 15, 2024

# Reporting Summary

Nature Portfolio wishes to improve the reproducibility of the work that we publish. This form provides structure for consistency and transparency in reporting. For further information on Nature Portfolio policies, see our Editorial Policies and the Editorial Policy Checklist.

## Statistics

For all statistical analyses, confirm that the following items are present in the figure legend, table legend, main text, or Methods section.

| n/a | Confirmed |
|---|---|
| ☐ | ☒ The exact sample size (*n*) for each experimental group/condition, given as a discrete number and unit of measurement |
| ☐ | ☒ A statement on whether measurements were taken from distinct samples or whether the same sample was measured repeatedly |
| ☐ | ☒ The statistical test(s) used AND whether they are one- or two-sided<br>*Only common tests should be described solely by name; describe more complex techniques in the Methods section.* |
| ☒ | ☐ A description of all covariates tested |
| ☒ | ☐ A description of any assumptions or corrections, such as tests of normality and adjustment for multiple comparisons |
| ☐ | ☒ A full description of the statistical parameters including central tendency (e.g. means) or other basic estimates (e.g. regression coefficient) AND variation (e.g. standard deviation) or associated estimates of uncertainty (e.g. confidence intervals) |
| ☐ | ☒ For null hypothesis testing, the test statistic (e.g. *F*, *t*, *r*) with confidence intervals, effect sizes, degrees of freedom and *P* value noted<br>*Give P values as exact values whenever suitable.* |
| ☒ | ☐ For Bayesian analysis, information on the choice of priors and Markov chain Monte Carlo settings |
| ☒ | ☐ For hierarchical and complex designs, identification of the appropriate level for tests and full reporting of outcomes |
| ☒ | ☐ Estimates of effect sizes (e.g. Cohen's *d*, Pearson's *r*), indicating how they were calculated |

*Our web collection on statistics for biologists contains articles on many of the points above.*

## Software and code

Policy information about availability of computer code

| | |
|---|---|
| Data collection | No softwares and codes were used to collect data except for the model simulation analysis. |
| Data analysis | All data analysis was conducted using Python Version 3.9, Matlab Version 2022b and ArcMap Version 10.6. The major codes and data for generating the main figures in the manuscript can be accessed on GitHub (https://github.com/szhuangGIS/Urbanization-Drought). |

For manuscripts utilizing custom algorithms or software that are central to the research but not yet described in published literature, software must be made available to editors and reviewers. We strongly encourage code deposition in a community repository (e.g. GitHub). See the Nature Portfolio guidelines for submitting code & software for further information.

## Data

Policy information about availability of data

All manuscripts must include a data availability statement. This statement should provide the following information, where applicable:

- Accession codes, unique identifiers, or web links for publicly available datasets
- A description of any restrictions on data availability
- For clinical datasets or third party data, please ensure that the statement adheres to our policy

All data used in this study is available and can be accessed in public repositories. GSOD and GHCN global in-situ meteorological data can be accessed at https://www.ncei.noaa.gov/data/global-summary-of-the-day/ and https://www.ncei.noaa.gov/data/global-historical-climatology-network-daily/. CMA meteorological data is available at http://data.cma.cn/en/?r=data/detail&dataCode=A.0012.0001. ECAD data is available at https://www.ecad.eu/dailydata/predefinedseries.php. ERA5-

Land and ERA5 products are obtained from https://cds.climate.copernicus.eu/cdsapp#!/dataset/reanalysis-era5-land?tab=form and https://cds.climate.copernicus.eu/cdsapp#!/dataset/reanalysis-era5-pressure-levels?tab=overview. CHIRPS precipitation can be retrieved at https://data.chc.ucsb.edu/products/CHIRPS-2.0/. CRU product is available at https://crudata.uea.ac.uk/cru/data/hrg/cru_ts_4.06/. CPC data can be accessed at https://downloads.psl.noaa.gov/Datasets/cpc_global_precip/. CMIP6 simulation data is obtained from https://esgf-node.llnl.gov/search/cmip6/. GISA2.0 product is released at https://zenodo.org/record/6476661. GUB data can be obtained at http://data.starcloud.pcl.ac.cn/zh/resource/14. Koppen climate classification product is provided by https://www.gloh2o.org/koppen. MCD12Q1 product are provided by https://e4ftl01.cr.usgs.gov/MOTA/MCD12Q1.061/.

## Human research participants

Policy information about studies involving human research participants and Sex and Gender in Research.

| | |
|---|---|
| Reporting on sex and gender | This study did not involve human research participants. |
| Population characteristics | This study did not involve human research participants. |
| Recruitment | This study did not involve human research participants. |
| Ethics oversight | This study did not involve human research participants. |

Note that full information on the approval of the study protocol must also be provided in the manuscript.

# Field-specific reporting

Please select the one below that is the best fit for your research. If you are not sure, read the appropriate sections before making your selection.

☐ Life sciences ☐ Behavioural & social sciences ☒ Ecological, evolutionary & environmental sciences

For a reference copy of the document with all sections, see nature.com/documents/nr-reporting-summary-flat.pdf

# Ecological, evolutionary & environmental sciences study design

All studies must disclose on these points even when the disclosure is negative.

| | |
|---|---|
| Study description | This study provides a quantitative analysis of the effects of urbanization on local drought development based on local observations and model simulations. By examining the spatial and temporal distributions of urbanization effects on each drought metric at global urban-rural pairs, we identify the major associations between urbanization and local drought. We also apply the Weather Research and Forecasting (WRF) high-resolution regional climate model to simulate local drought under highly urbanized and non-urbanized scenarios in six representative cities spread across each continent. Subsequently, we delve into the potential mechanisms underlying these urbanization effects. The findings enhance our understanding of the role of urbanization in shaping drought patterns—a critical step towards sustainable urban development. |
| Research sample | Most data used in this study was collected from international community, such as NOAA, ECMWF, and CMIP6. All the dataset can be access by the public. The global impervious data and urban boundary data were obtained from published papers (Huang et al., 2022; Li et al., 2020). |
| Sampling strategy | This study was performed at a global scale. The selection of recent four decades as study period mainly considered the rapid urban expansion over this period, highlight the urbanization induced effects. The Sen's Slope and Mann-Kendall trend test were applied to examine the trends. For model simulation, we selected six representative urban regions across various continents due to their significant urban expansion and historical severe drought occurrences. |
| Data collection | All data used in this study was downloaded from the corresponding websites without any software. |
| Timing and spatial scale | For historical analysis, the data was collected from 1980 to 2020 with daily temporal resolution. For future projection, the collected CMIP6 data ranged from 2015 to 2050 with both daily and monthly time scale. The study area for station-based analysis included the regions with available in-situ measurements in the globe. The study area for model simulation consisted of six representative urban regions across various continents, including Yangtze River Delta in Asia, Madrid in Europe, Chicago in North America, São Paulo in South America, Cape Town in Africa, and Sydney in Australia. |
| Data exclusions | No collected data was excluded from analysis. |
| Reproducibility | The code for each experiment and analysis was ran multiple times to verify the reproducibility. |
| Randomization | Randomization is not relevant for this study as all data analysis was based on observational and widely adopted remotely sensed and reanalysis products. |
| Blinding | No blinding process was used in this study since there are no participants that can be influenced. |

Did the study involve field work? ☐ Yes ☒ No

# Reporting for specific materials, systems and methods

We require information from authors about some types of materials, experimental systems and methods used in many studies. Here, indicate whether each material, system or method listed is relevant to your study. If you are not sure if a list item applies to your research, read the appropriate section before selecting a response.

## Materials & experimental systems

| n/a | Involved in the study |
|---|---|
| ☒ | ☐ Antibodies |
| ☒ | ☐ Eukaryotic cell lines |
| ☒ | ☐ Palaeontology and archaeology |
| ☒ | ☐ Animals and other organisms |
| ☒ | ☐ Clinical data |
| ☒ | ☐ Dual use research of concern |

## Methods

| n/a | Involved in the study |
|---|---|
| ☒ | ☐ ChIP-seq |
| ☒ | ☐ Flow cytometry |
| ☒ | ☐ MRI-based neuroimaging |